Anisotropy in BaFe$_2$Se$_3$ single crystals with double chains of FeSe tetrahedra

Hechang Lei,[1] Hyejin Ryu,[1,2] Anatoly I. Frenkel,[3] and C. Petrovic[1,2]

[1]*Condensed Matter Physics and Materials Science Department,*
Brookhaven National Laboratory, Upton, NY 11973, USA

[2]*Department of Physics and Astronomy, State University of New York at Stony Brook, Stony Brook, NY 11794, USA*

[3]*Physics Department, Yeshiva University, 245 Lexington Avenue, New York, NY 10016, USA*

(Dated: December 8, 2011)

We studied the anisotropy in physical properties of Ba$_{1.00(4)}$Fe$_{1.9(1)}$Se$_{3.1(1)}$ single crystals. BaFe$_2$Se$_3$ is a semiconductor below 300 K. Magnetization measurements show that there is a crossover from a short-range antiferromangetic (AFM) correlations at room temperature to a long-range AFM order with $T_N = 255$ K. The anisotropy of magnetization is consistent with the previous neutron results. This crossover is supported by the heat capacity measurement where the phase-transition peak is absent at 255 K. The superconducting transition at about 10 K is likely due to the small amount of β-FeSe impurities.

I. INTRODUCTION

Since the discovery of iron-based superconductors,[1] iron pnictide and chalcogenide materials have stimulated great interest. All iron-based superconductors show some structural similarity. From the initially discovered LaFeAsO$_{1-x}$F$_x$ to very recently reported K$_x$Fe$_{2-y}$Se$_2$ two-dimensional (2D) FePn or FeCh (Pn = pnictogens, Ch = chalcogens) tetrahedron layers are the common structural ingredient probably related to high temperature superconductivity.[1−5] However, the mechanism of superconductivity and its relation to the crystal structure motifs in these systems is still under debate. In order to fully understand the nature of the superconductivity, study of materials containing similar building blocks related to these systems is of significant interest.

On the other hand, the dimensionality of magnetic interactions and electronic transport is another important factor which will influence Fermi surface topology and magnetic ground state. For example, CaFe$_4$As$_3$ is a compound which is closely related to iron-based superconductors but has a different dimensionality and spatial arrangement of similar FePn(Ch) local structural units. It contains an open three-dimensional (3D) channellike network of shared FeAs tetrahedra with Ca atoms in the channels that run along the b axis of the orthorhombic cell.[6] CaFe$_4$As$_3$ exhibits Fermi-liquid behavior with enhanced electron-electron correlations and antiferromagnetic (AFM) long range order without superconductivity above 1.8 K.[6,7]Another structurally related material is BaFe$_2$Se$_3$ which contains one-dimensional (1D) double chains of edge shared Fe-Se tetrahedra along the b-axis.[8] Studies of magnetic properties indicate that there is a crossover from short range AFM correlation to long range AFM order at around 250 K. However, the existence of a superconducting transition at the low temperature is still controversial.[9,10]

In this work, we report the detailed characterization of anisotropic physical properties and local crystal structure of Ba$_{1.00(4)}$Fe$_{1.9(1)}$Se$_{3.1(1)}$ single crystals. We show

that this material is a semiconductor with long-range antiferromagnetic (AFM) order below $T_N = 255$ K.

II. EXPERIMENT

Single crystals of BaFe$_2$Se$_3$ were grown by self-flux method with nominal composition Ba:Fe:Se = 1:2:3. Ba pieces, Fe powder and Se shot were mixed and put into the carbon crucible, then sealed into the quartz tube with partial pressure of argon. The quartz tube was annealed at 1150 °C for 24 h for homogenization, and then the ampoule was slowly cooled down to 750 °C with about 6 °C/hour. Finally, the furnace was shut down and the ampoule was cooled down to room temperature naturally. Single crystals with typical size 5×2×1 mm^3 can be grown. The powder X-ray diffraction (XRD) spectra were taken with Cu K$_\alpha$ radiation $\lambda = 1.5418$ Å using a Rigaku miniflex x-ray machine. The orientation of crystal is determined using Bruker SMART APEX II single crystal x-ray diffractometer. The average stoichiometry was determined by examination of multiple points using an energy-dispersive x-ray spectroscopy (EDX) in a JEOL JSM-6500 scanning electron microscope. The X-ray absorption spectra of the Fe and Se K-edges were taken in transmission mode on powder samples of BaFe$_2$Se$_3$ at the X18A beamline of the National Synchrotron Light Source. Standard procedure was used to extract the X-ray absorption near edge structure (XANES) and extended x-ray absorption fine-structure (EXAFS) from the absorption spectrum.[11] Standard Fe and Se metal foils and FeO, Fe$_2$O$_3$ and Fe$_3$O$_4$ oxide powders were used for energy calibration and also for evaluating the valence states of Fe and Se ions. Electrical transport measurements were performed using a four-probe configuration. Thin Pt wires were attached to electrical contacts made of silver paste. Electrical transport, heat capacity, and magnetization measurements were carried out in Quantum Design PPMS-9 and MPMS-XL5.
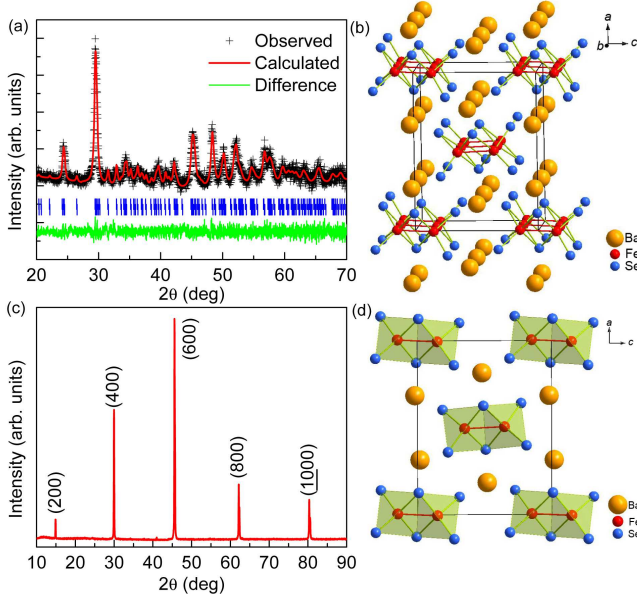
FIG. 1. (a) Powder XRD patterns of $BaFe_2Se_3$. (b) Crystal structure of $BaFe_2Se_3$. The big orange, small red and medium blue balls represent Ba, Fe and Se ions. (c) Single crystal XRD of $BaFe_2Se_3$. (d) The arrangement of double chains of edge-sharing Fe-Se tetrahedra along b axis.

III. RESULTS AND DISCUSSION

Powder XRD result and structural refinements of $BaFe_2Se_3$ using Rietica[12] (Fig. 1(a)) indicate that all reflections can be indexed in the Pnma space group. The refined lattice parameters are a = 11.940(2) Å, b=5.444(1) Å, and c = 9.174(1) Å, consistent with the values reported in literature.[9,10] The crystal structure of $BaFe_2Se_3$ (Fig. 1(b)) can be depicted as alternate stacking of Fe-Se layers and Ba cations along the crystallographic a axis, similar to $K_xFe_{2-y}Se_2$.[5] However, in the Fe-Se plane, Fe-Se tetrahedra do not connect each other along two planar directions to form a two-dimensional (2D) infinite layer. Instead, they are broken along the c-axis periodically and only one dimensional (1D) double chains of edge shared Fe-Se tetrahedra propagate along the b-axis.. The double-chains are separated by Ba^{2+} ions and are slightly tilted off the bc-plane. The tilting directions are opposite between the two neighboring layers as shown in Fig. 1(d). The shape of $BaFe_2Se_3$ crystal is long plate like. The XRD pattern of a $BaFe_2Se_3$ crystal (Fig. 1(c)) reveals that the crystal surface is normal to the a axis with the plate-shaped surface parallel to the bc-plane. Moreover, the b axis is along the long direction of crystal in the bc-plane. The EDX spectrum of a single crystal confirms the presence of Ba, Fe and Se. The average atomic ratios determined from EDX are Ba:Fe:Se = 1.00(4):1.9(1):3.1(1), close to the expected stoichiometric $BaFe_2Se_3$ ratio. Hence, there are no vacancies on either Ba or Fe sites, which is different from $K_xFe_{2-y}Se_2$.[5,13]

The features of Fe K-edge XANES spectrum of $BaFe_2Se_3$ (Fig. 2(a)) are similar to $FeSe_x$.[14] The pre-peak A ($\sim$ 7112.5 eV) is due to either dipole or quadrupole 1s $\longrightarrow$ 3d transitions. The shoulder B with maximum absorption jump at $\sim$ 7118.4 eV can be ascribed to the 1s $\longrightarrow$ 4p transition. When compared to the spectrum of FeO, the shoulder B is located at the lower energy side, suggesting that the valence of Fe is slightly smaller than 2+. The valence of Fe is evaluated by linear interpolation of the energy of $BaFe_2Se_3$ with those of standards (Fe foil (metallic Fe), FeO (Fe^{2+}) and Fe_2O_3 (Fe^{3+})). From the peak of first-derivative spectra corresponding to the maximum absorption jump we obtain $\sim$ 1.87+ for Fe valence, which is close to the value for $FeSe_x$.[14] On the other hand, there are two features for Se K-edge XANES spectrum of $BaFe_2Se_3$ (Fig. 2b). The feature C is mainly due to the 1s $\longrightarrow$ 4p dipole transition and the broad hump D should be a multiple scattering of the photoelectron with the near neighbors.[15] By extrapolating the maximum absorption jumps of Se ($\sim$ 12659.2 eV) and SeO_2 ($\sim$ 12662 eV),[14] we estimate $\sim$ -1.98 for the Se valence, consistent with the formal value of Se ion (2-). For the Fe site, the nearest neighbors are four Se atoms ($1\times$Se(I), $2\times$Se(II) and $1\times$Se(III)) with four different distances close to $\sim$ 2.418 Å and the next nearest neighbors are three Fe atoms with almost the same distance ($\sim$ 2.723 Å).[8] From the joint analysis of Fe and Se edges EXAFS data using a single bond distance for Fe-Se and Fe-Fe, and by fitting the k range 3.2-18.4 Å^{-1} for Fe K-edge and 2-14 Å^{-1} for Se K-edge (main panels and insets of Fig. 2(c) and (d)), the fitted average Fe-Se and Fe-Fe bond lengths are d_{Fe-Se} = 2.428(5) Å and d_{Fe-Fe} = 2.71(5) Å. This is consistent with the reported values.[8]

Temperature dependence of the resistivity $\rho(T)$ of $BaFe_2Se_3$ crystal for $\mu_0H = 0$ and 9 T indicates that this material is a semiconductor in measured temperature region. (Fig. 3). The room-temperature value $\rho(300K)$ is about 17 $\Omega\cdot$cm, which is much larger than in $BaFe_2S_3$ ($\sim$ 0.35 $\Omega\cdot$cm).[16] Fits of the $\rho(T)$ at high temperature using the thermal activation model $\rho = \rho_0 \exp(E_a/k_BT)$, where ρ_0 is a prefactor, E_a is thermal activated energy and k_B is Boltzmann's constant, gives E_a = 0.178(1) eV in the temperature range above 170 K (inset in Fig. 3), which is also much larger than in $BaFe_2S_3$.[16,17] The larger room-temperature resistivity and E_a can be ascribed to the increase of structural distortion which might localize the carriers and increase the band gap when compared to $BaFe_2S_3$.[8] For $BaFe_2S_3$, bond lengths are almost identical for all four Fe-S bonds, in contrast to very different bond lengths for $BaFe_2Se_3$. Moreover, the Fe-Fe bond distances in a single chain are identical for $BaFe_2S_3$ whereas they are different for $BaFe_2Se_3$, where the longer and shorter bonds alternately connect along the b axis. All structural features imply that in the former compound the coordination polyhedron is more symmetric than in the latter. It should be noted that the shorter Fe-Fe bond in $BaFe_2S_3$ may also have some contribution
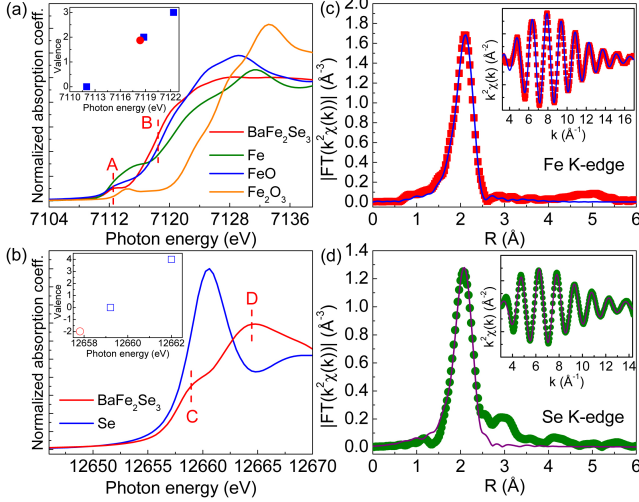
FIG. 2. (a) Fe K-edge XANES spectra of $BaFe_2Se_3$, Fe, FeO, and Fe_2O_3 measured at 300 K. The inset shows the valence states of Fe calculated from the first derivative of the XANES spectra. FT magnitudes of the EXAFS oscillations (symbols) for Fe K-edge (c) and Se K-edge (d). The model fits are shown as solid lines. The FTs are not corrected for the phase shifts and represent raw experimental data. Insets of (c) and (d) filtered EXAFS (symbols) with k-space model fits (solid line).
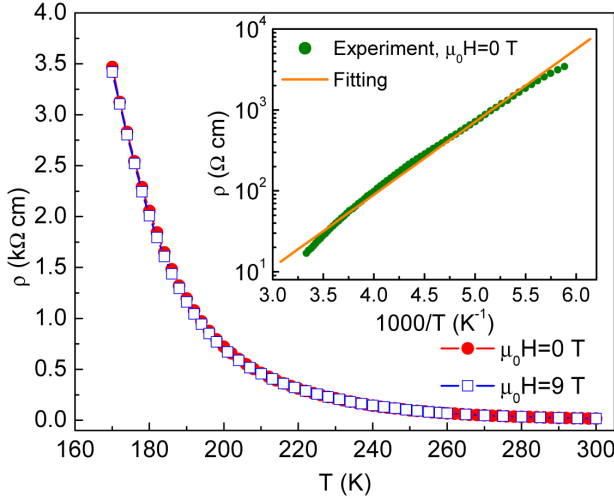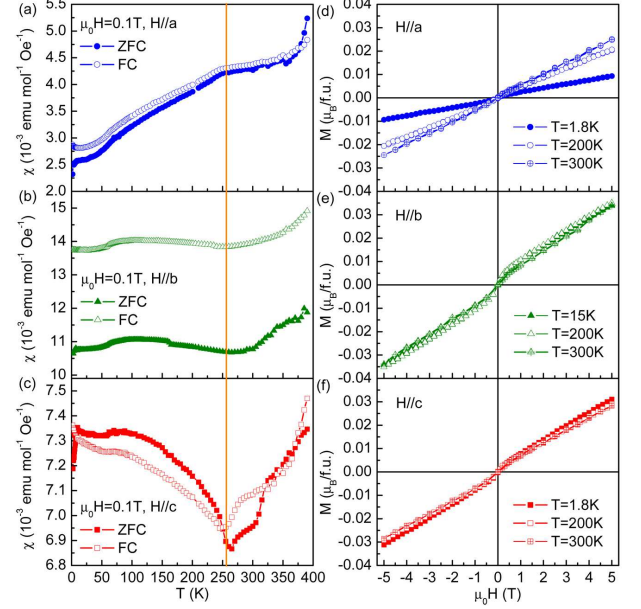

FIG. 4. (a) Temperature dependence of DC magnetic susceptibility $\chi(T)$ below 300 K under ZFC and FC modes with the applied field $\mu_0 H = 0.1$ T along (a) a, (b) b and (c) c axis. Isothermal magnetization hysteresis loops M(H) for (d) H∥a, (e) H∥b and (f) H∥c at various temperatures.

FIG. 3. Temperature dependence of the resistivity $\rho(T)$ of the $BaFe_2Se_3$ crystal with $\mu_0 H = 0$ (closed red circle) and 9 T (open blue square, H∥c). Inset: Fitting result of $\rho(T)$ at zero field using thermal activation model where the red line is the fitting curve.

to higher conductivity. On the other hand, when compared to $BaFe_2S_3$ which exhibits negative magnetoresistance (MR) below 25 K,[16] there is no obvious MR in $BaFe_2Se_3$ as shown in Fig. 3.

Temperature dependence of dc magnetic susceptibility $\chi(T)$ of $BaFe_2Se_3$ single crystal (Fig. 4(a), (b) and (c)) can not be fitted using Curie-Weiss law up to 390 K. It

decreases with decreasing temperature for all field directions (H∥a,b, and c). It suggests that there is AFM interaction up to 390 K, in agreement with neutron results that found short range correlations (SRC).[9,10] Another characteristic in $\chi(T)$ curves is a transition appearing at about 255 K for all three field directions, which is ascribed to a crossover from short-range AFM correlation to long-range AFM order.[9,10] It should be noted that the absolute $\chi_a(T)$ is much smaller than $\chi_b(T)$ and $\chi_c(T)$. Nevertheless, similar to H∥b, a Curie-like upturn in susceptibility is seen below 255 K for H∥c, while a faster drop is seen below 255 K for H∥a. It suggests that the easy-axis of magnetization direction is a axis. According to mean-field theory for collinear antiferromagnet, magnetic susceptibility along the easy-axis direction goes to zero for T → 0 whereas perpendicular to the easy-axis magnetization direction is nearly constant below T_N. This is consistent with the neutron results.[9,10] The small positive value of $\chi_a(T \to 0)$ is probably due to the presence of a van Vleck paramagnetism. A large diversity of susceptibilities between H∥a, H∥b and H∥c persisting up to 390 K suggests that there may be an intriguing anisotropy of SRC in the system. On the other hand, when the magnetic field was applied along the c axis, there is no obvious hysteresis between ZFC and FC measurements. The lack of hysteresis suggests that the ferromagnetic component of magnetic interactions between the Fe chains along the c axis is very weak. This can be ascribed to the large Fe-Fe (or ferromagnetic Fe4 plaquette) interchain distance ($d_{Fe-Fe}^{interchain} \sim 6.441$ Å).[8] In contrast, for H∥b, the ZFC
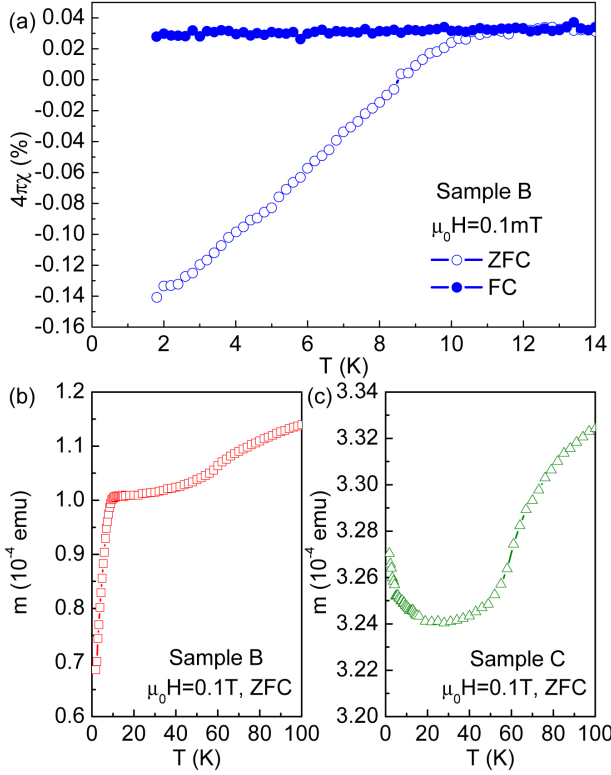
FIG. 5. (a) $\chi(T)$ of sample B below 15 K under ZFC and FC modes with $\mu_0 H = 0.1$ mT. $\chi(T)$ below 100 K under ZFC mode with $\mu_0 H = 0.1$ T for (b) sample B and (c) sample C.

and FC measurements exhibit significant hysteresis due to the fact of short Fe-Fe (or ferromagnetic Fe4 plaquette) intrachain distance ($d_{Fe-Fe}^{intrachain} \sim 2.720$ Å and 2.727 Å),[8] resulting in strong magnetic interaction. The hysteresis between the ZFC and FC curves extends up to 390 K, suggesting that this intrachain interaction exists at temperatures above the long range order.

Isothermal M(H) for H∥a, H∥b and H∥c (Fig. 4(d), (e) and (f)) at various temperature show that there is no hysteresis for all three field directions which confirm the AFM order in the system and exclude the ferromagnetic impurities. For H∥a, the slopes of M(H) increase with increasing temperature but for other two directions, M(H) curves are almost unchanged, consistent with the M(T) results. Moreover, the slopes of M(H) are H∥b > H∥c > H∥a for all of measured temperatures, corresponding to the increase of paramagnetic moment when magnetic field is rotated from a towards c and then towards the b axis as shown Fig. 4(a), (b) and (c).

On the other hand, there is a small drop at about 10 K. This is also observed in previous report and might correspond to the superconducting transition.[9] In order to clarify whether this transition is extrinsic or intrinsic, we measured other two samples from the same batch. As shown in Fig. 5 (a) and (b), sample B exhibits similar drop at about 10 K for $\mu_0 H = 0.1$ mT and 0.1 T, but the superconducting volume fraction is only about 0.15% at 1.8 K for $\mu_0 H = 0.1$ mT. On the other hand, sample
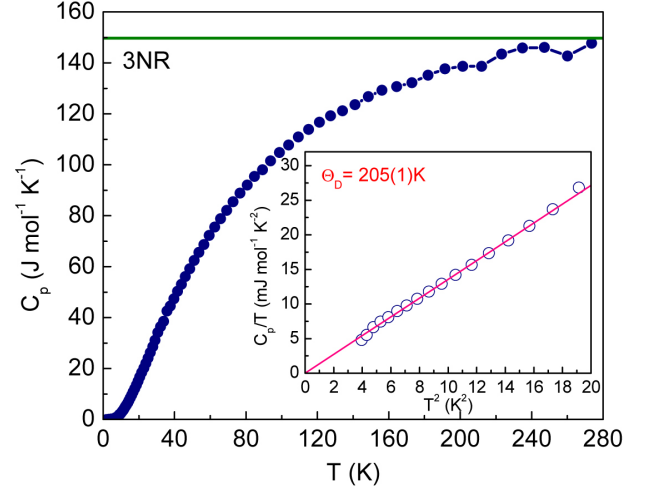

FIG. 6. Temperature dependence of heat capacity for $BaFe_2Se_3$ crystal. The green solid line represents the classical value according to Dulong-Petit law at high temperature. Inset: the low-temperature specific-heat data in the plot of C_p/T vs T^2. The red solid line is the fitting curves using formula $C_p/T = \beta T^2$.

C does not show any drop below 15 K for $\mu_0 H = 0.1$ T. These results imply that this superconducting transition should be extrinsic and coming from residual β-FeSe in the melt. Moreover, the transition temperature (~ 10 K) is close to the T_c of β-FeSe (~ 8.5 K and up to ~ 36.7 K at 8.9 GPa).[18] Thus, a small drop at about 10 K might be ascribed to the residual amount of β-FeSe impurities.

The heat capacity C_p of $BaFe_2Se_3$ crystal approaches the classic value of 3NR at 300 K, where N is the atomic number in the chemical formula (N = 6) and R is the gas constant (R = 8.314 J mol^{-1} K^{-1}), consistent with the Dulong-Petit law (Fig. 6). At the low temperature, $C_p(T)$ curve can be fitted solely by a cubic term βT^3 (inset of Fig. 6). From the fitted value of $\beta = 1.357(6)$ mJ mol^{-1} K^{-4}, the Debye temperature is estimated to be $\Theta_D = 205(1)$ K using the formula $\Theta_D = (12\pi^4 NR/5\beta)^{1/3}$. This is slightly smaller than Θ_D of $K_xFe_{2-y}Se_2$, which might be due to the larger atomic mass of Ba than K.[19] On the other hand, there is no λ-type anomaly for $BaFe_2Se_3$ at the temperature of magnetic transitions ($T_N = 255$ K). This can be ascribed to the overwhelming release of magnetic entropy due to existence of SRC above the long range order at T_N.[10] This is also consistent with the absence of Curie-Weiss law in M(T) (Fig. 4(a), (b) and (c)).

IV. CONCLUSION

In summary, we studied the physical properties of $Ba_{1.00(4)}Fe_{1.9(1)}Se_{3.1(1)}$ single crystals with 1D double chains of edge shared Fe-Se tetrahedra parallel to the b-axis. Composition analysis indicates that all crystallographic sites are fully occupied. XANES result shows

that the valence of Fe is about 1.87+. Taken together with transport, magnetic and thermodynamic properties, this indicates that the $BaFe_2Se_3$ is a semiconductor with a short-range AFM correlation at the room temperature and a long-range AFM order below 255 K. The anisotropy of magnetization is consistent with magnetic structure determined from neutron results previously. This is rather similar to parent materials of Fe based superconductors, however the absence of appreciable conductivity coincides with the absence of connected infinite 2D Fe-Se planar tetrahedra.

V.   ACKNOWLEDGEMENT

[1] Y. Kamihara, T. Watanabe, M. Hirano, and H. Hosono, J. Am. Chem. Soc. **130**, 3296 (2008).

[2] M. Rotter, M. Tegel, and D. Johrendt, Phys. Rev. Lett. **101**, 107006 (2008).

[3] X. C. Wang, Q. Q. Liu, Y. X. Lv, W. B. Gao, L. X. Yang, R. C. Yu, F. Y. Li ,and C. Q. Jin, Solid State Commun. **148**, 538 (2008).

[4] F. C. Hsu, J. Y. Luo, K. W. Yeh, T. K. Chen, T. W. Huang, P. M. Wu, Y. C. Lee, Y. L. Huang, Y. Y. Chu, D. C. Yan, and M. K. Wu, Proc. Natl. Acad. Sci. USA **105**, 14262 (2008).

[5] J. Guo, S. Jin, G. Wang, S. Wang, K. Zhu, T. Zhou, M. He, and X. Chen, Phys. Rev. B **82**, 180520(R) (2010).

[6] I. Todorov, D. Y. Chung, C. D. Malliakas, Q. Li, T. Bakas, A. Douvalis, G. Trimarchi, K. Gray, J. F. Mitchell, A. J. Freeman, and M. G. Kanatzidis, J. Am. Chem. Soc. **131**, 5405 (2009).

[7] L. L. Zhao, T. H. Yi, J. C. Fettinger, S. M. Kauzlarich, and E. Morosan, Phys. Rev. B **80**, 020404(R) (2009).

[8] H. Y. Hong and H. Steinfink, J. Solid State Chem. **5**, 93 (1972).

[9] A. Krzton-Maziopa, E. Pomjakushina, V. Pomjakushin, D. Sheptyakov, D. Chernyshov, V. Svitlyk, and K. Conder, J. Phys.: Condens. Matter **23**, 402201 (2011).

[10] J. M. Caron, J. R. Neilson, D. C. Miller, A. Llobet, and T. M. McQueen, Phys. Rev. B **84**, 180409(R) (2011).

[11] R. Prins and D. Koningsberger, X-ray Absorption: Principles, Applications, Techniques of EXAFS, SEXAFS, XANES, Wiley, New York (1988).

[12] Hunter B. (1998) "Rietica - A visual Rietveld program", International Union of Crystallography Commission on Powder Diffraction Newsletter No. 20, (Summer) http://www.rietica.org

[13] H. C. Lei and C. Petrovic, Phys. Rev. B **83**, 184504 (2011).

[14] C. L. Chen, S. M. Rao, C. L. Dong, J. L. Chen, T. W. Huang, B. H. Mok, M. C. Ling, W. C. Wang, C. L. Chang, T. S. Chan, J. F. Lee, J.-H. Guo, and M. K. Wu, EPL, 93 47003 (2011).

[15] B. Joseph, A. Iadecola, L. Simonelli, Y. Mizuguchi, Y. Takano, T. Mizokawa, and N. L. Saini, J. Phys.: Condens. Matter **22**, 485702 (2010).

[16] Z. S. Gönen, P. Fournier, V. Smolyaninova, R. Greene, F. M. Araujo-Moreira, and B. Eichhorn, Chem. Mater. **12**, 3331 (2000).

[17] W. M. Reiff, I. E. Grey, A. Fan, Z. Eliezer, and H. Steinfink, J. Solid State Chem. **13**, 32 (1975).

[18] S. Medvedev, T. M. McQueen, I. A. Troyan, T. Palasyuk, M. I. Eremets, R. J. Cava, S. Naghavi, F. Casper, V. Ksenofontov, G.Wortmann, and C. Felser, Nature Mater. **8** 630 (2009).

[19] B. Zeng, B. Shen, G. F. Chen, J. B. He, D. M. Wang, C. H. Li, and H. H. Wen, Phys. Rev. B **83**, 144511 (2011).